Interannual to Interdecadal Variability in the Japan Sea Based on a New Gridded Upper Water Temperature Dataset

SHOSHIRO MINOBE

Division of Earth and Planetary Sciences, Graduate School of Science, Hokkaido University, Hokkaido, Sapporo, Japan, and Frontier Research System for Global Change, Yokohama City, Kanagawa, Japan

AKINORI SAKO* AND MAKOTO NAKAMURA+

Division of Earth and Planetary Sciences, Graduate School of Science, Hokkaido University, Hokkaido, Sapporo, Japan

(Manuscript received 16 August 2002, in final form 31 March 2004)

ABSTRACT

A new gridded water temperature dataset of upper 400-m depths (0, 50, 100, 200, 300, and 400 m) for the Japan Sea (or East Sea) is produced by using an optimal interpolation technique from 1930 to 1996, based on oceanographic observations collected in the World Ocean Database 1998. The temperature data are analyzed by a complex empirical orthogonal function (CEOF) with six levels combined using the data for a period from 1957 to 1996, during which most of gridded data are available. Before calculating the CEOFs, low-pass or high-pass filters (cutoff period at 7 yr) are applied to separate interannual and decadal temperature changes, respectively. One interannual and two decadal CEOF modes are identified. The interannual first CEOF mode is characterized by the energetic variability around and south of the subpolar front in the western Japan Sea, accompanied by northward and northeastward phase propagations emanating from the Tsushima Strait. The decadal first CEOF mode exhibits a broad structure prevailing over the whole Japan Sea, but large amplitudes are trapped by the subpolar front, with 60°–90° phase lags between the northeastern and southwestern Japan Sea. The decadal second CEOF mode has a localized structure with strong correlations in the Yamato Basin. The relation between the atmosphere and ocean is analyzed by a correlation analysis of wintertime sea level pressures (SLPs) onto the temporal coefficients of the CEOF modes. The interannual first CEOF mode is accompanied by the SLP anomalies over the western North Pacific Ocean with steep SLP gradients over the Japan Sea, suggesting that this mode is forced by local wind anomalies associated with the SLP changes over the western North Pacific. The decadal first CEOF mode is likely to be caused by changes of the east Asian winter monsoon due to the SLP variability of the northern part of the Siberian high, which is closely associated with the decadal fluctuations of the Arctic Oscillation and the North Atlantic Oscillation. The second decadal CEOF mode is accompanied by high SLP correlations over the central North Pacific associated with strength changes of Aleutian lows, suggestive of remote forcing from the central North Pacific.

1. Introduction

The Japan Sea or East Sea has been called ''a world ocean in miniature'' (Ichiye 1984) because it contains the features and elements of a world ocean, including subtropical and subpolar waters, western boundary currents and their separation. Knowledge of the Japan Sea is, therefore, useful for understanding processes in the World Ocean. For interannual to interdecadal changes of the Japan Sea, several papers have reported some aspects of interesting variations as described below, but the nature of those variations was not yet fully documented.

On interannual time scales, variations with a 2–3-yr period and those with about 6-yr period were reported. Toba et al. (1982) noted a 2–3-yr variation in the transport of the Tsushima Warm Current. Also, Isoda (1994) reported a biennial spectral peak in SST data along 134°E. Consistently, Hirose and Ostrovskii (2000) detected a quasi-biennial oscillation of sea level displacements observed by Ocean Topography Experiment (TOPEX)/Poseidon altimetry. In contrast to the 2–3-yr oscillations reported in recent papers (except for Toba et al. 1982), earlier papers showed occurrences of 6-yr oscillations. Miita and Tawara (1984) found a 6-yr oscillation in surface and subsurface water temperatures at the Tsushima Strait. Naganuma (1985) also reported

* Current affiliation: Alpha Hydraulic Engineering Consultants, Sapporo, Japan.

+ Current affiliation: IBM Global Service, Japan Solution and Services Company, Sapporo, Japan.

Corresponding author address: Shoshiro Minobe, Division of Earth and Planetary Sciences, Graduate School of Science, Hokkaido University, Hokkaido, Sapporo 060-0810, Japan.
E-mail: minobe@ep.sci.hodudai.ac.jp

6-yr variability in the volume transport of the Tsushima Warm Current at the Tsushima Strait. Watanabe et al. (1986), analyzing Japanese coastal SST data, showed that a 6-yr signal propagated from the southwest to the northeast direction along the Japanese coast taking 1–2 yr.

On decadal time scales, Watanabe et al. (1986) found an oscillatory SST variation with a period of about 10 yr north of 40°N in the Japanese coastal SST data. In addition to the coastal analysis using data before the 1970s by Watanabe et al. (1986), Isoda (1994) reported a consistent decadal SST variation from an SST analysis along 134°E from the 1970s to the 1980s. Also, Chu et al. (1998) showed cold anomalies prevailing over the subpolar front from 1984 to 1987, based on gridded SST data during a period from 1982 to 1994. Senjyu (1999) found variability in sea level displacements on a time scale of roughly 20 yr along the Japanese coast on both the Japan Sea side and the North Pacific Ocean side.

For none of these interesting interannual to interdecadal variations in the Japan Sea, however, have three-dimensional spatial structures been identified. Therefore, the purpose of this paper is to describe the spatiotemporal structures of interannual to interdecadal variations of water temperatures in the Japan Sea. In order to attain this purpose, we have produced a new gridded water temperature dataset in the upper 400-m depth of the Japan Sea. This dataset is the first gridded dataset of subsurface water temperature anomalies with a spatial resolution high enough for analyses of year-to-year variations in the Japan Sea.

This paper is organized as follows. Background information of the Japan Sea useful for understanding of interannual to interdecadal variability is described in section 2. The oceanographic data used for the gridded data and gridding methodologies are described in section 3, whereas the method of analysis for the gridded data and associated atmospheric data are explained in section 4. The interannual and interdecadal water temperature variations are documented in section 5. Relations between the oceanic and atmospheric variations are examined in section 6. Discussion and conclusions are presented in section 7.

2. Background

The Japan Sea is a rather large (1×10^6 km^2) and deep midlatitude marginal sea in the western North Pacific with an average depth over 1500 m and a maximum depth over 3500 m (Fig. 1). The Japan Sea is connected by four shallow and narrow straits to the North Pacific, East China Sea, and Okhotsk Sea.

In the upper 200 m, waters in the northern Japan Sea are relatively cold and fresh, and waters in the southern Japan Sea are warm and saline, separated by the ''subpolar front'' around 39°–40°N. Most water in the Japan Sea is supplied from the Kuroshio and the East China Sea through the Tsushima Strait, while waters of the Japan Sea flow out from the Tsugaru and Soya Straits (Isobe 1999). A recent study by Chu et al. (2001) estimated the transports at the Tsushima, Tugaru, and Soya straits as 2.3, 1.4, and 0.9 Sv (1 Sv $\equiv 10^6$ m^3 s^{-1}), respectively. The warm and saline inflows from the Tsushima Strait are mainly divided into the northward-flowing East Korean Warm Current along the Korean coast and the northeastward-flowing Japan Nearshore Branch along the Japanese coast (Yoon 1982a,b,c; Kawabe 1982a,b; Hase et al. 1999). The strong winter cooling associated with the east Asian winter monsoon contribute to cold-water temperatures in the northern part of the Japan Sea and formation of the Liman Current (e.g., Martin and Kawase 1998), and cold and fresh waters are also supplied from the Okhotsk Sea through the Mamiya Strait (or Tartarky Strait) to the northern Japan Sea. The eastward-flowing waters of the subpolar front are fed by the Liman Cold Current and East Korean Warm Current after their separation from the western boundary.

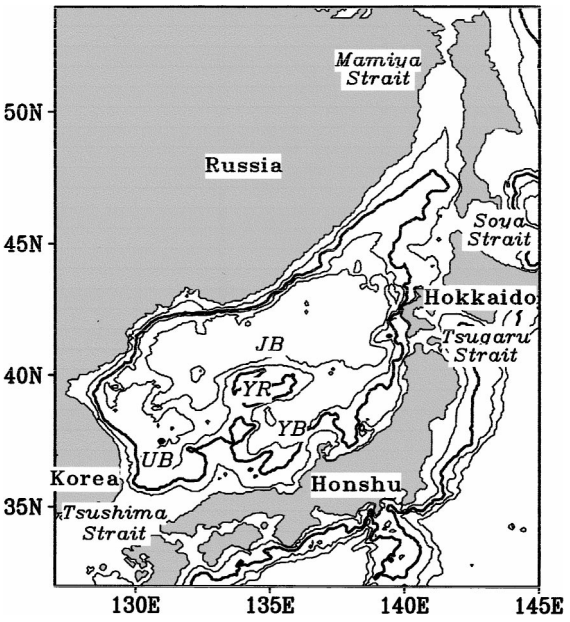

FIG. 1. Bottom topography in the Sea of Japan. The contour levels are at depths of 200, 1000, 2000, and 3000 m. The thick contour denotes the 1000-m depth. Labels JB, UB, and YB denote Japan, Ulleung, and Yamato Basins, respectively, and YR denotes Yamato Rise.

In contrast to the prominent differences across the subpolar front in the upper 200-m depth, below 300–400-m depths the water properties are quite uniform with potential temperatures colder than 0.6°C and salinities of about 34.06 practical salinity unit (psu). This homogeneous water is called the Japan Sea Proper Water (JSPW; Uda 1934; Sudo 1986; Kim and Kim 1999). Just above the JSPW, Japan/East Sea Intermediate Water (J/ESIW), which is characterized by salinity minimum and high oxygen with potential temperatures of 1°–5°C

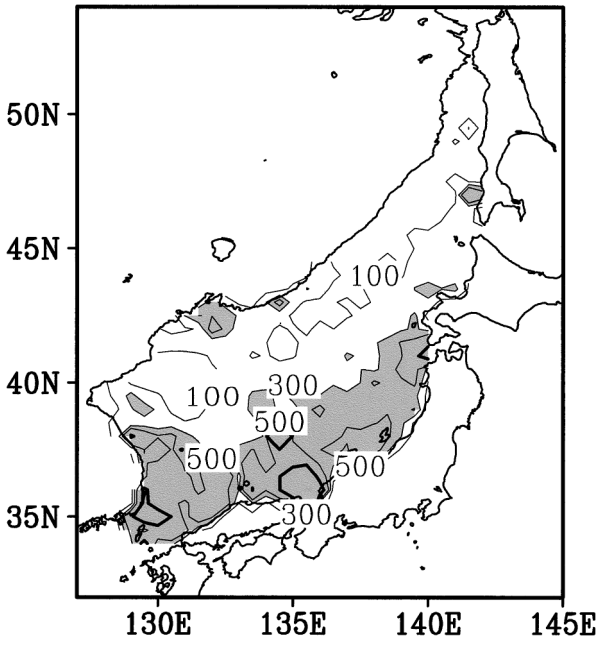

FIG. 2. Number of observations per 0.5° × 0.5° bin for the whole observation period (1930–96). Contour levels are for 100, 300, 500, and 1000 observations, and the thick contour denotes 1000. Gray shading indicates the regions where observation numbers are larger than 500.

(Kim and Chung 1984; Kim and Kim 1999), prevails over the western Japan Sea, while High-Salinity Intermediate Water (HSIW), which is characterized by high salinity and high oxygen with potential temperatures of 0.6°–5°C (Kim and Kim 1999), is distributed in the eastern Japan Sea north of the subpolar front.

3. Oceanographic observation data and gridding method

The temperature profiles collected in the World Ocean Database (WOD; Levitus et al. 1998) are used to produce a gridded temperature dataset. There are 151 740 temperature profiles in the Sea of Japan. Observation densities are large in the Japanese side and small in the Siberian side (Fig. 2). As explained later, the bias arising from the observation density distribution is not likely to be sufficiently substantial to seriously influence the major results of the present paper.

We employ an optimal interpolation (OI) technique to produce the gridded water temperature anomalies on a monthly, 0.5° × 0.5° grid at six depth levels of 0, 50, 100, 200, 300, and 400 m. The OI methodology was developed by Gandin (1965) and others and has been applied in oceanographic data gridding (e.g., White 1995).

Before gridding the data, we applied the following quality control. We first excluded the data that are flagged as erroneous in WOD, colder than −2°C, or located at depths deeper than the bottom depth. Then, we temporarily calculated climatological monthly means at each depth and for each month on a 0.5° × 0.5° grid by a Gaussian filter whose *e*-folding scale and influence radius are 100 and 200 km, respectively. The seasonal cycle is estimated based on the monthly mean temperatures by fitting these to annual and semiannual cycles, yielding a monthly climatology. For each observation, a climatological temperature is estimated by an interpolation from the monthly climatology, and an anomaly is defined as the difference of the observed temperature from the interpolated climatological temperature. A datum whose anomaly is larger than 2.5 times the standard deviation of anomalies at the corresponding grid point is removed from further analyses. This quality-control scheme removes 3.7% of the surface data and 5.3% at 400-m depth. After removing these data, the monthly climatology and temperature anomalies from the climatology are recalculated using the same method described above.

TABLE 1. Parameters used for OI gridding. Here S/N is the signal-to-noise ratio, D_x and D_y are the zonal and meridional decorrelation scale in degrees (longitude and latitude, respectively), and D_T is the temporal decorrelation scale in months.

Depth (m)	S/N	D_x	D_y	D_t
0	0.7	7.5	4.6	1.5
50	1.0	2.5	1.9	5.9
100	1.0	2.4	1.7	9.8
200	1.3	2.0	1.8	9.7
300	1.7	2.6	2.8	8.0
400	1.8	3.7	4.3	7.5

In an OI, observed data are assumed to be a superposition of signal and noise, and the signal values are estimated and gridded. The spatiotemporal structure of the signal, which is expressed by autocorrelation functions, and signal-to-noise ratios should be estimated before gridding.

A signal-to-noise ratio, defined as a square root of the ratio of the signal variance to the noise variance, is estimated from anomaly temperatures at each depth as follows. We calculated signal variance by averaging covariance for all pairs of individual observations separated by less than 50 km in the same month and year, but excluding an observation paired with it. Here, we have assumed that a lag smaller than 50 km and one month can be ignored for a signal. On the other hand, total (signal plus noise) variance is given by the autovariance, which is equivalent to the covariance for observations paired with it, and was excluded for the estimation of the signal variance. Thus, we obtained the noise variance by subtracting the signal variance from the total variance. Observed signal-to-noise ratios from the surface to the 400-m depth are summarized in Table 1.

To estimate the autocorrelation functions for the signal and subsequent gridding, we use so-called superobservations (White 1995). A superobservation is a substitutional datum representing raw anomalies over a 0.5° × 0.5° bin in a month and in a year at each depth. The

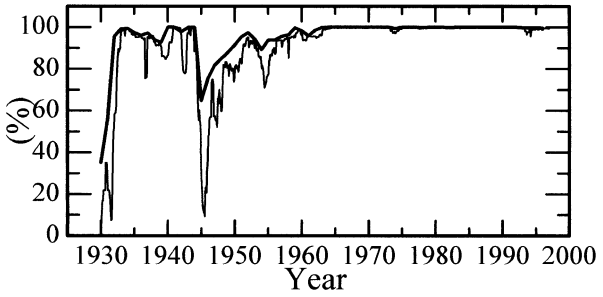

FIG. 3. Percentages of available grid number of upper-layer temperatures of the Japan Sea for the monthly data (thin line) and annually averaged data (thick line). An annual average value is calculated for a grid that has one or more available monthly data for a calender year.

value of the superobservation is given by the average of raw anomalies in the bin, and location is defined at the center of gravity of the raw observations. The use of superobservations significantly reduces the computation amount and also the complexity of program coding.

In the present OI, the autocorrelation function for the signal is assumed to have a Gaussian form, as

$$r(d_x, d_y, d_t) = \exp[-(d_x/D_x)^2 - (d_y/D_y)^2 - (d_t/D_t)^2], \quad (1)$$

where r is the autocorrelation function, d_x and d_y are the zonal and meridional distances, respectively, d_t is the temporal differences, and D_x, D_y, and D_t are the respective decorrelation scales. It is noteworthy that the correlation structure of (1) is conservatively assumed not to involve phase lags, and hence phase propagations will not be imposed in the gridded temperatures artificially. Autocorrelation coefficients are calculated using the superobservations, and the decorrelation scales are estimated by fitting (1) to the observed autocorrelations. The spatial decorrelation scales at depth are much smaller than those at the surface, while the opposite tendency is found for the temporal scales (Table 1).

The gridded temperature anomalies are estimated from the superobservations with the OI parameters by a standard OI method as described by White (1995) in detail. In the case in which there is no observation within the *e*-folding temporal and spatial distance from the center of a grid, the gridded anomalies are treated as unavailable. After gridded anomalies are calculated by the OI, the climatology and anomaly fields are recalculated. Figure 3 shows the time series of available grid percentages for the resultant gridded temperature anomalies. High grid availability occurs after the mid-1950s and from the mid-1930s to the early 1940s, with a lack of gridded data during World War II in the 1940s.

Figure 4 shows climatological annual mean temperature fields at respective depths. The subpolar front is evident from 50–100-m depths as strong temperature gradients. As depth increases, the subpolar front shifts toward the south. The subpolar front is less prominent at the surface, mainly because of the summertime surface heating; in the winter season the surface front is as evident as at other depths (not shown). Strong temperature gradients are also observed just north of the Honshu coast from 129° to 135°E at 50- and 100-m depths, corresponding to the Japan Nearshore Branch. Waters of temperatures approximately in the range from 0.6° to 5°C correspond to J/ESIW in the western Japan Sea, and to HSIW in the eastern Japan Sea, respectively (Kim and Chung 1984; Kim and Kim 1999).

Figure 5 shows that the temperature anomaly variances are large along the subpolar front from the surface to 100-m depth. At 200-m depth, the strong variability is found in the Ulleung and Yamato Basins. At deeper 300- and 400-m depths, the variances distribute more uniformly over the Japan Sea. These features are reflected in the results of the CEOF analyses (section 5). The region of small subsurface variances at 50 and 100 m correspond to the region of the intermediate waters shown by 0.6°–5°C temperatures in the climatology. This correspondence implies a physical relationship between the interannual variance and climatology. The intermediate waters are hypothesized to be formed north of the subpolar front (Kim and Kim 1999). Changes of the wintertime cooling strength may change the formation rate of intermediate waters rather than the temperature changes, resulting in relatively small temperature changes north of the subpolar front. Although the smaller number of observations in the northern Japan Sea shown in Fig. 2 might be responsible for the small variance there, the physically consistent relation between the variance and climatology suggests that this bias does not seriously skew the analysis.

4. Method of analysis and atmospheric data

We use complex empirical orthogonal functions (CEOFs) to describe the interannual to interdecadal variability of upper water temperatures in the Japan Sea for the analysis period from 1957 to the end of the record (1996) for which gridded data are available without interruptions for most grids (Fig. 3). The CEOFs are calculated based on a covariance matrix for the annually averaged temperature anomalies at all six levels (0–400 m) combined. For the present combined CEOF analysis, the temperature anomalies are weighted by the square roots of respective layer thickness. A linear trend for the analysis period is removed at respective grid points, and high-pass or low-pass filters with a cutoff period of 7 yr are applied to the detrended data in order to know differences between the structures of interannual and decadal variations. For simplicity, a CEOF mode calculated for high-pass (low pass) filtered data is denoted as an interannual (decadal) CEOF mode hereinafter. Before applying the fast Fourier transform (FFT) for the temperature data for filtering and Hilbert transform, we extended time series by 20% at the beginning and end,

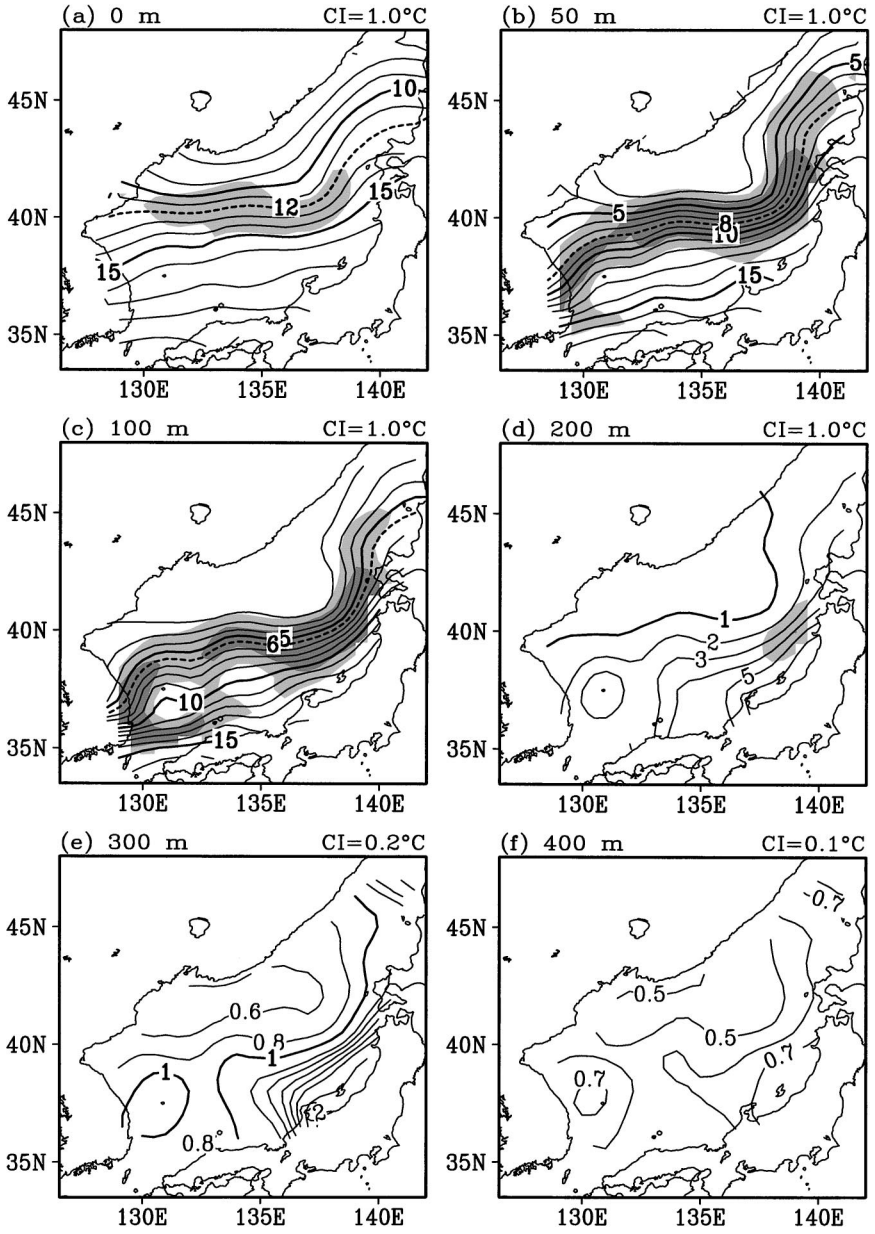

FIG. 4. Climatological annual mean temperature (contours) with the magnitude of the mean temperature gradient (shaded). The contour interval (CI) is given at the top of each panel, and thick contours indicates 1°, 5°, 10°, and 15°C. For representing the subpolar front, a contour in the middle of the steep temperature gradients is chosen and is shown by a thick dashed contour of 12°, 8°, and 6°C in (a), (b), and (c), respectively. Dark and medium gray shades indicate the region where the temperature gradient is larger than 3×10^{-2} and 2×10^{-2} °C km^{-1}, respectively.

using an autoregressive model based on a maximum entropy method on the order of 30% of the number of years. Then, a data taper for the FFT, a cosine taper of 10% of the full (observed plus extended) record, was applied. Thus, the taper does not modify the observed portion of the record, and hence the covariance matrix was calculated for the whole length of the analysis period. Grid points with no annually averaged value during the analysis period (1957–96) are excluded from the CEOF calculation. The use of monthly data instead of the annually averaged data reproduces essentially the same results, but with a larger number of unavailable grids as expected from Fig. 3.

We also examined (real) EOFs, but CEOFs are likely to be more relevant to describe water temperature variations in the Japan Sea; the first and second (real) EOFs for low-pass filtered temperature data and associated principal components (PCs) exhibited an out-of-phase

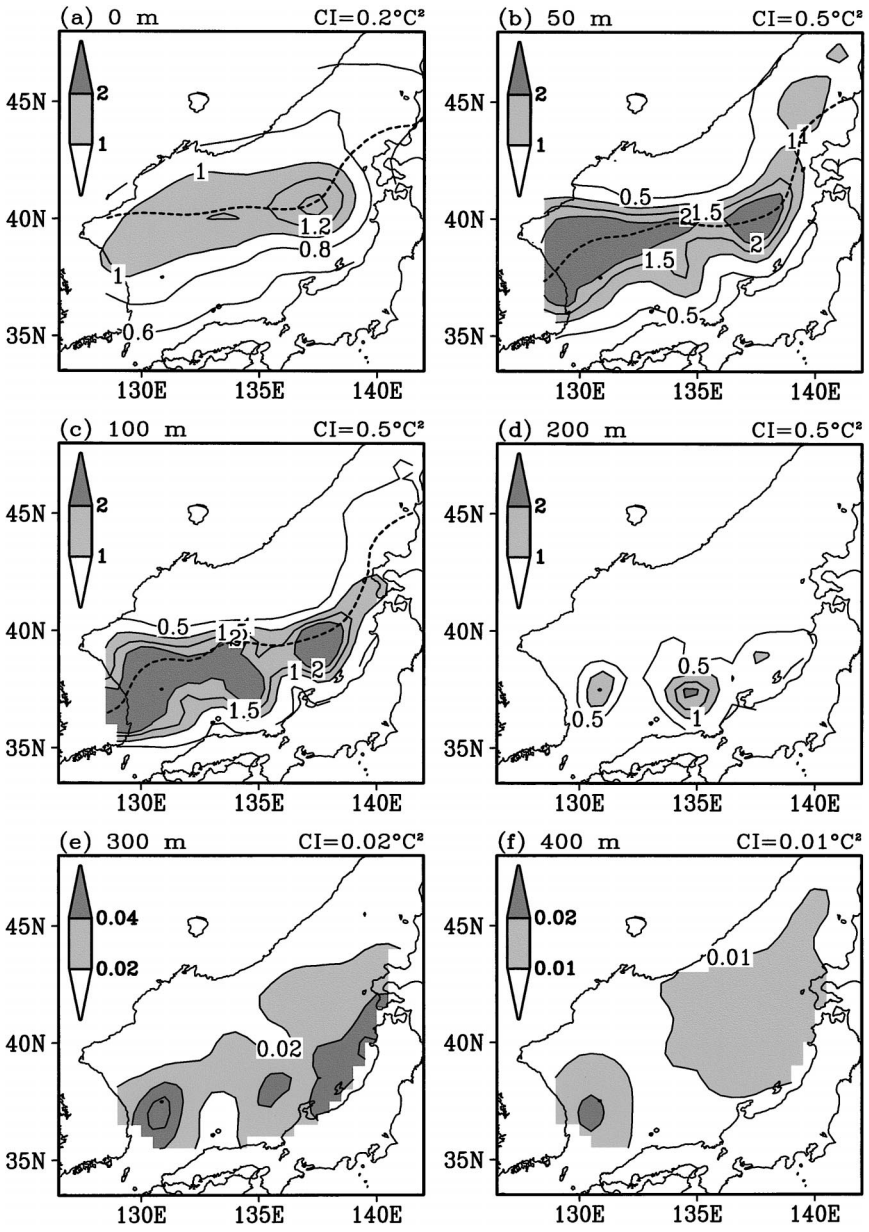

FIG. 5. Variance of temperature anomalies from climatological monthly means from 1957 to 1996. Contour intervals are denoted at the top of each panel, and shading is explained by the bars on the left. The thick dashed contours in (a), (b), and (c) are the isotherms corresponding to the subpolar front at each depth as shown in Fig. 4.

relation with a 90° phase difference with comparable explained variances (not shown), suggesting that the first two EOFs are not physically independent, but are two aspects of a single phenomenon. In such a case, it is reasonable to employ CEOFs instead of EOFs.

If we calculate the CEOFs without prefiltering, the first two CEOF modes calculated from unfiltered data closely resemble the first two decadal CEOF modes, but the first interannual mode is not reproduced by the unfiltered CEOF analysis. As will be shown later, the interannual first mode is statistically meaningful and also physically reliable from a comparison with the atmospheric parameters. Therefore, CEOF analysis with interannual or decadal filtering is an appropriate methodology to extract physically interesting modes.

In order to investigate atmospheric variability corresponding to the oceanic changes, we examine a sea level pressure (SLP) dataset by a correlation analysis onto the PCs or the temporal coefficients of the CEOFs. The monthly SLP data used in the present study are an updated version of the Trenberth and Paolino (1980) archives for the period of record 1899–2001.

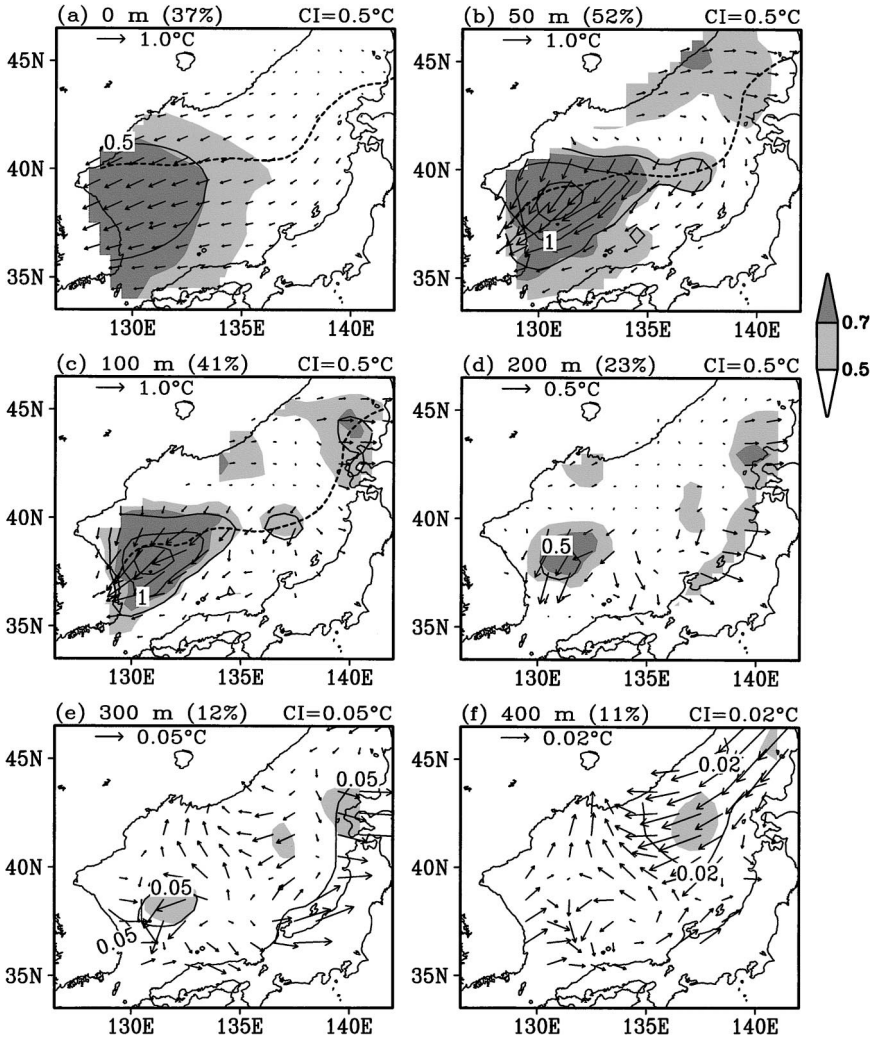

FIG. 6. Spatial patterns of the interannual first CEOF mode of water temperatures. The contours indicate the amplitudes of CEOFs (°C), and the CI is given at the top of each panel. Dark (medium) gray shading indicates the region where correlation coefficients are higher than 0.7 (0.5) between the temperatures and the PC-1. The amplitudes are also indicated by the length of the arrows according to the scale in the respective panels. The phases are indicated by the direction of the arrows: an arrow pointing to the right indicates 0° phase, an arrow pointing to the top of the page is 90°, etc. (phase increases in the direction of arrow rotating counterclockwise). The direction of phase increase is the direction of phase propagation.

5. Oceanic variations

The explained variances of the first two CEOF modes on interannual (period < 7 yr) time scales are 42% and 12%. The first mode is well separated from the second mode according to the rule of thumb by North et al. (1982), suggesting that this mode is statistically meaningful. In addition to the small explained variance of the second mode, because the spatial pattern of the second mode is not well organized, we focus on the first mode for further description.

Figure 6 shows the spatial pattern of the interannual CEOF-1. This mode explains about 40%–50% variance from the surface to 100-m depth, whereas the ratio of the explained variance rapidly decreases as depth further increases. The maximum amplitudes of the CEOF-1 occur in the western Japan Sea around and south of the subpolar front from the surface to 200-m depth. This suggests that this mode is strongly associated with the East Korean Warm Current and its extension. The maximal amplitude of 1.9°C is observed at 100-m depth, where the correlation coefficient also marks its maximal value of 0.95. The spatial phase distribution suggests a weak northward and northeastward propagation from Tsushima Strait to 40°N and to 135°E. Moreover, the structures at 50- and 100-m depth indicate that the variability associated with this mode further penetrates

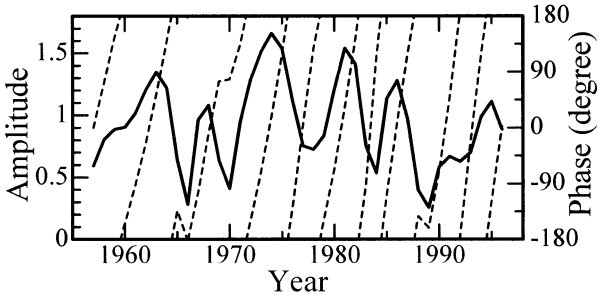

FIG. 7. Amplitude (solid line) and phase (dashed line) of the first principal component (PC-1) or temporal coefficient of the interannual CEOF-1 shown in Fig. 6. The PC is normalized by its standard deviation.

eastward from 135°E along the subpolar front. Secondary maxima of amplitudes are observed in the northern Japan Sea off the Siberian coast at 50-m depth, and off the Hokkaido coast at 100-m depth. At these secondary maxima, the phases are roughly 180° out of phase with the phases around Tsushima Strait.

The corresponding PC-1 shows that the period of the oscillation in the earlier half of the record (5–6 yr) is generally longer than in the latter half (2–3 yr; Fig. 7). This periodicity change is consistent with the aforementioned fact that the earlier papers using the data until the 1970s generally reported the occurrences of 6-yr oscillations (e.g., Miita and Tawara 1984; Naganuma 1985; Watanabe et al. 1986), but biennial variations were documented by more recent papers (e.g., Isoda 1994; Hirose and Ostrovskii 2000). It is also noteworthy that although Watanabe et al. (1986) reported a northeastward SST propagation with a 6-yr periodicity along the Japanese coast, the present results have revealed that the propagation along the Japanese coast is a minor aspect of the basinwide phenomenon presented by the interannual CEOF-1.

For the first three decadal CEOF modes, the ratios of the explained variance are 60%, 20%, and 8%. The rule of thumb by North et al. (1982) suggests that the second mode is not well separated statistically from the first mode. As will be shown in the next section, however, the decadal second mode is accompanied by interesting atmospheric circulation anomalies as well as the first mode. This suggests that the decadal second mode is also useful for understanding the variability in the Japan Sea. Thus, we describe closely these two modes.

Similar to the interannual CEOF-1, the decadal CEOF-1 explains the high ratios of variances (60%–70%) from the surface to 100-m depth. The spatial pattern of CEOF-1 at 50- and 100-m depths has strong amplitudes (>1°C) trapped by the subpolar front, suggestive of the meridional shift of the front, and the maximal amplitude reaches 2.1°C at 100-m depth in a transition area between Yamato Basin and Japan Basin (Fig. 8). The correlation coefficients are generally large in the northeastern Japan Sea, where correlation coefficients higher than 0.9 (0.7) are observed down to 300-m (400 m) depths. In the northeastern Japan Sea, the phases increase as depth increases from 100- to 400-m depth, indicating that temperature anomalies propagate downward. The phases at 50- and 100-m depths may be viewed as consisting of two groups in the northeastern and southwestern Japan Sea. The phases in the southwestern Japan Sea lead the northeastern ones by 60°–90° (Fig. 8), indicating a lag of several years, combined with the 10–20-yr time scale shown by 2.5 cycles of phase rotation of the PC-1 for the 40-yr record (Fig. 9).

The spatial structure of the second mode exhibits a more localized structure than that of the first mode (Fig. 10). In this structure, Yamato Basin seems to be a key region, since correlations higher than 0.7 occur in the basin from the surface to 400-m depth. It is noteworthy that the Yamato Basin is one of the most well observed regions in the Japan Sea (Fig. 2). The largest amplitude of 1.1°C is observed at 100-m depth off Korea around 38°N, where correlations are about 0.6. The phase distributions from 50- to 300-m depths indicate that the temperature anomalies in the Yamato Basin lead those off Korea. The PC-2 indicates that the time scale of this mode is 10–20 yr (not shown).

6. Ocean–atmosphere relation

Here we examine large-scale atmospheric variations relating to the Japan Sea changes described in the previous section. The relations are evaluated by a correlation analysis of wintertime (December–February) SLPs onto the PCs for the Japan Sea water temperatures. We applied the aforementioned high-pass or low-pass filters to the SLP data before calculating correlations for consistency. Also, a Hilbert transform is applied to the SLP data, so that correlations are again expressed by complex values. If summertime (June–August) SLPs are used instead of the wintertime SLPs, smaller correlations are obtained in all cases. This suggests that the wintertime atmospheric forcings more strongly influence water temperatures than the summertime ones.

Figure 11 shows correlation coefficients of the wintertime SLPs onto the interannual PC-1. The correlations are large (above 0.7) over the western North Pacific with a steep gradient of correlations over the Japan Sea. The phases of the high correlations (arrow directions in Fig. 11) over the western North Pacific are roughly the same as the phases of CEOF-1 around the Tsushima Strait (arrow directions in Fig. 6), from which temperature anomalies propagate to the inside of the Japan Sea as described above. A time series comparison between the reconstructed water temperature at the Tsushima Strait and area-averaged SLPs over the western North Pacific indicates that the covariability between them holds throughout the record regardless of the aforementioned dominant periodicity of 2–3 or 5–6 yr (Fig. 12). This in-phase relation and the SLP gradients over the Japan Sea suggest that the geostrophic wind anomalies are closely related with the temperature

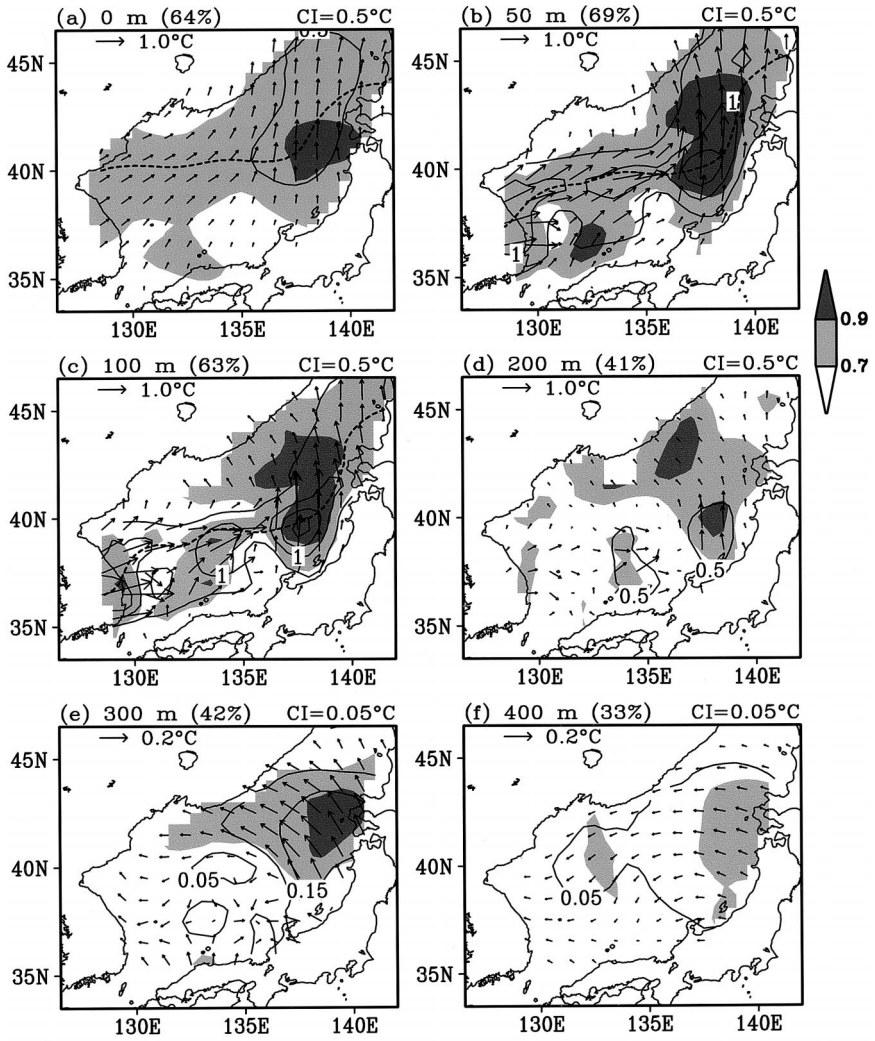

FIG. 8. Same as Fig. 6, but for the decadal first CEOF mode.

changes in the Japan Sea. Consistently, a simultaneous regression map of wintertime wind stress anomalies of the National Centers for Environmental Prediction (NCEP)–National Center for Atmospheric Research (NCAR) reanalysis (Kalnay et al. 1996) onto the reconstructed water temperature time series shows that the warmer (cold) temperatures are accompanied by the clockwise (counterclockwise) wind stress anomalies over the Japan Sea (Fig. 13). The wind anomalies near the Eurasia coast are in direction almost parallel to the coastline. This suggests that the temperature changes are associated with Kelvin or shelf wave modes forced by alongshore wind anomalies. The northward propagation direction of the CEOF-1 is, however, opposite to the phase-propagation direction of Kelvin and shelf waves, which should propagate southward along the Korean coast, suggesting that another mechanism, such as advection of temperature anomalies by mean currents, is necessary to explain the whole structure of the interannual first mode.

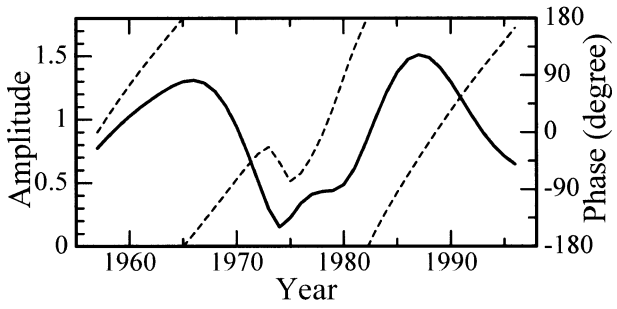

FIG. 9. Same as Fig. 7, but for the decadal PC-1.

For the decadal PC-1, large correlation coefficients of SLPs prevail over the Eurasian continent north of 50°N (Fig. 14), where phases of SLPs are approximately opposite to the phases of the water temperatures in the northeastern Japan Sea (Fig. 8). The location of large

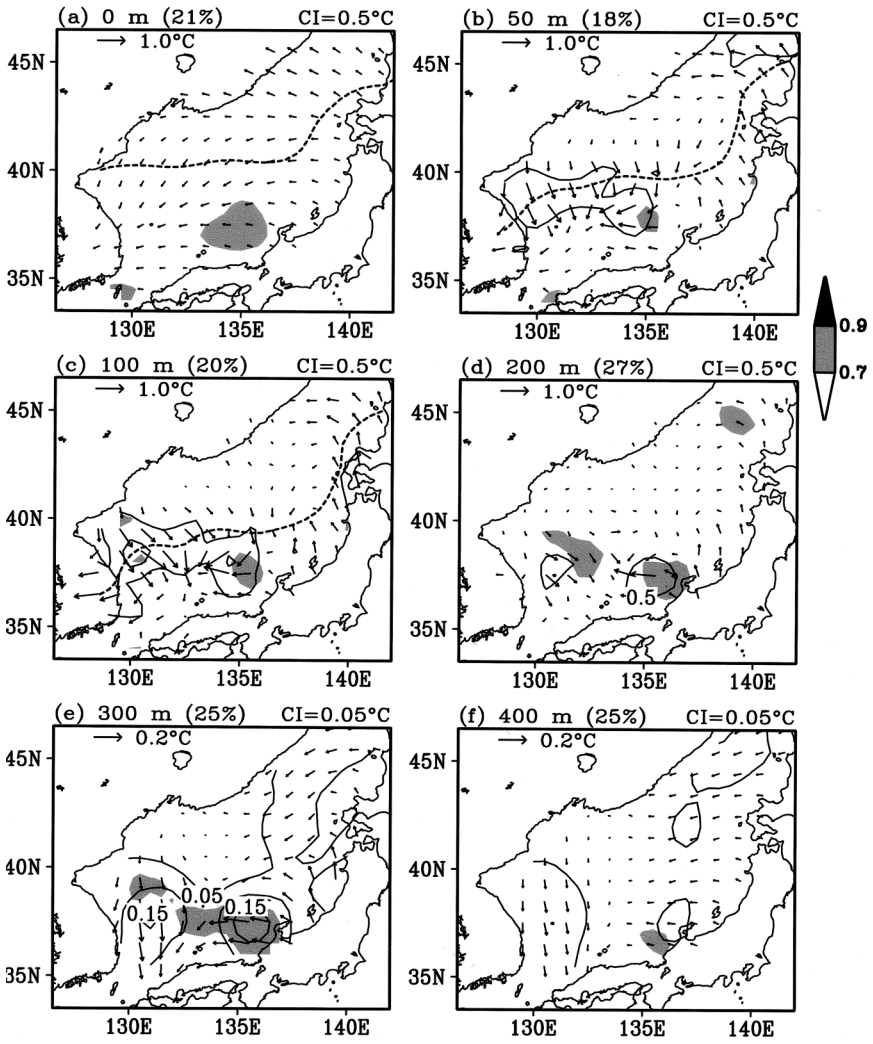

FIG. 10. Same as Fig. 8, but for the decadal second mode.

correlations corresponds to the northern half of the climatological wintertime Siberian high. It is known that SLP changes over this region strongly influence the east Asian winter monsoon (e.g., Gong et al. 2001). Consistent with the out-of-phase relation between the SLPs and water temperatures, a stronger Siberian high is expected to induce a severer winter monsoon involving stronger outbreaks from the Siberian coast to the Japan Sea, resulting in cold water temperature anomalies.

The reconstructed water temperature for the decadal first mode at the amplitude maximum at 100-m depth exhibits consistent covariability with low-pass-filtered time series of area-averaged SLPs over northern Eurasia [Fig. 15 (top)], though the peak and trough of the water temperature time series in the 1970s are less prominent than those of the SLP. It is noteworthy that the cold anomalies in the reconstructed temperature in the mid-1980s are consistent with the cold-SST period from 1984 to 1987 reported by Chu et al. (1998). Gong et al. (2001) noted a close relation between the year-to-year variability of the Siberian high and the Arctic Oscillation (AO) proposed by Thompson and Wallace (1998). Consistent with this, decadal variability similar to that of the water temperatures is also observed in the wintertime AO and North Atlantic Oscillation (NAO) indices after 1965, though similar decadal AO/NAO variability was absent before that [Fig. 15 (bottom)]. The quasi-decadal variability of the NAO, which is shared by the AO, was reported by Hurrell (1995), and its influence to eastern Asia and the North Pacific was discussed by Xie et al. (1999). Consequently, the decadal variability of the northeastern Japan Sea is dominated by the decadal oscillation of the northern half of the Siberian high, which is related strongly but not totally with the decadal variability of the AO/NAO.

The phase difference between the southwestern and northeastern Japan Sea for the decadal first mode noted in the previous section is not likely to be a direct con-

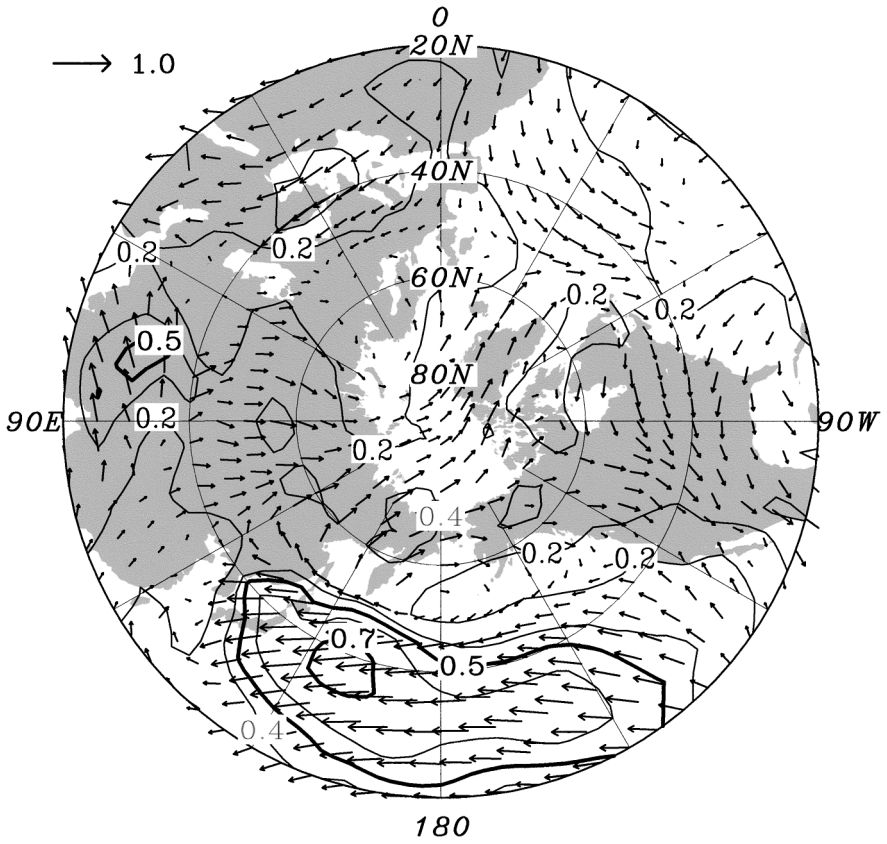

FIG. 11. Correlation map of the wintertime SLPs onto the interannual PC-1 shown in Fig. 7. The contours and arrow lengths indicate absolute values of the complex correlations, and the directions of arrows indicate the phases. The contour levels are 0.2, 0.4, 0.5, 0.6, and 0.7. The thick contours denote 0.5 and 0.7, which correspond to the shades in Fig. 6. The phase convention is the same as Fig. 6, and hence an angle between an arrow in the present figure and an arrow in Fig. 6 indicates the phase difference; the arrows pointing in the same direction are in phase.

sequence of the atmospheric cooling associated with the strength changes of the east Asian winter monsoon. Based on a simple model consisting of two boxes corresponding to the northern and southern Japan Sea, Isoda (1999) proposed that a decadal cooling in the northern Japan Sea induces a roughly 90° delayed heating in the southern Japan Sea through the following mechanism. Atmospheric cooling in the northern box enhances the meridional temperature differences between the boxes. The increased temperature differences induce a larger eastward geostrophic transport, which is assumed to be equal to a warm-water transport from the Tsushima Strait to the southern box, resulting in a lagged warming in the southern box. The proposed phase relation between the northern and southern boxes is somewhat similar to the observed relation between the northeastern and southwestern Japan Sea. However, the two box model lacks some important physical processes; for example, transports at Tsushima Strait should be subject to local adjustment processes as shown by Nof (1993) and Ohshima (1994). Consequently, in order to examine whether Isoda's (1999) hypothesis is appropriate for the decadal first mode, we need to await further developments of numerical and theoretical studies, which allow treating realistic responses of the Japan Sea to the atmospheric cooling, including the adjustment processes at straits.

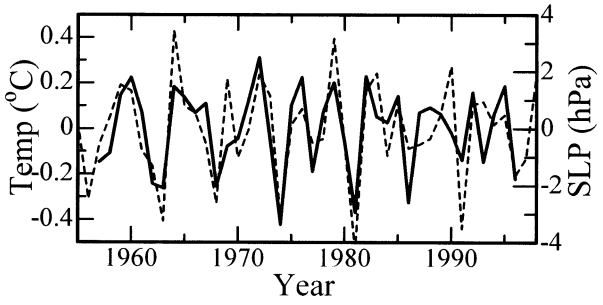

FIG. 12. Time series of reconstructed water temperature at 35°N, 130°E and 100-m depth for the interannual CEOF-1 (solid line), and high-pass-filtered SLPs averaged over the western North Pacific (35°–45°N, 135°–170°E) (dashed line).

Correlation coefficients of SLPs onto the decadal PC-2 are large over the central North Pacific (Fig. 16). The

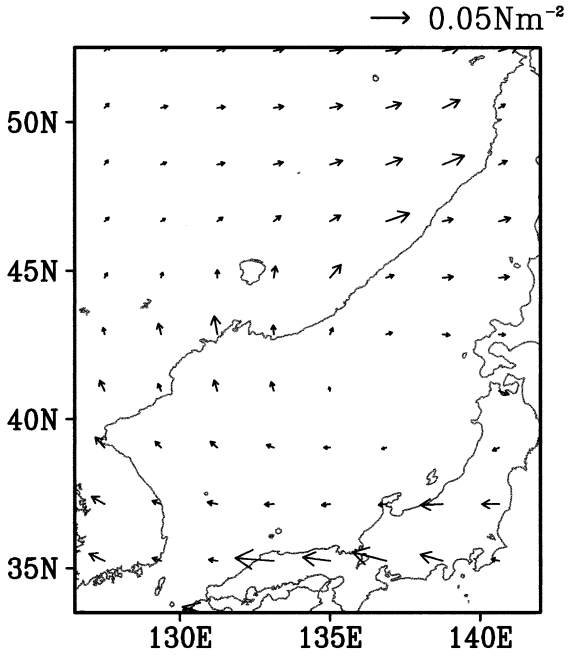

FIG. 13. Regression map of the wintertime surface wind stress onto the reconstructed water temperature time series shown in Fig. 12.

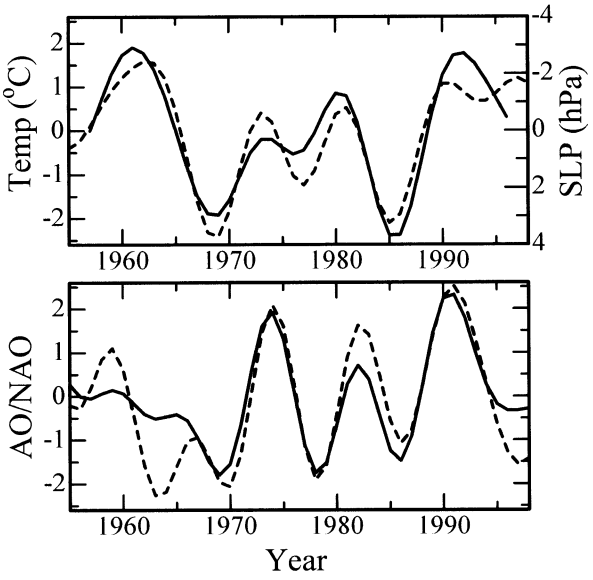

FIG. 15. (top) Same as Fig. 12 but for the reconstructed temperature at 40°N, 138°E and 100-m depth for the decadal CEOF-1 (solid line) and low-pass-filtered wintertime SLPs averaged over northern Eurasia (50°–70°N, 50°–140°E) (dashed line). (bottom) Low-pass-filtered wintertime Arctic Oscillation index (solid line) and North Atlantic Oscillation index (dashed line) in an arbitrary unit.

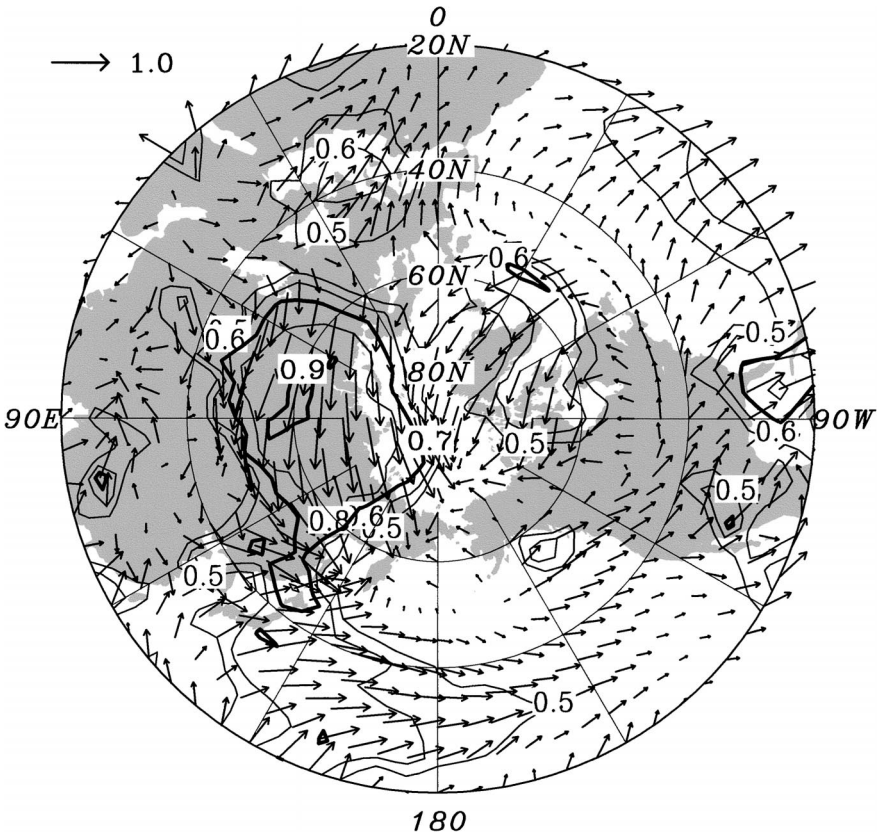

FIG. 14. Same as Fig. 11, but for the decadal first CEOF mode. Contour levels are 0.5, 0.6, 0.7, 0.8, and 0.9. The thick contours denote 0.7 and 0.9, which correspond to the shades in Fig. 8.

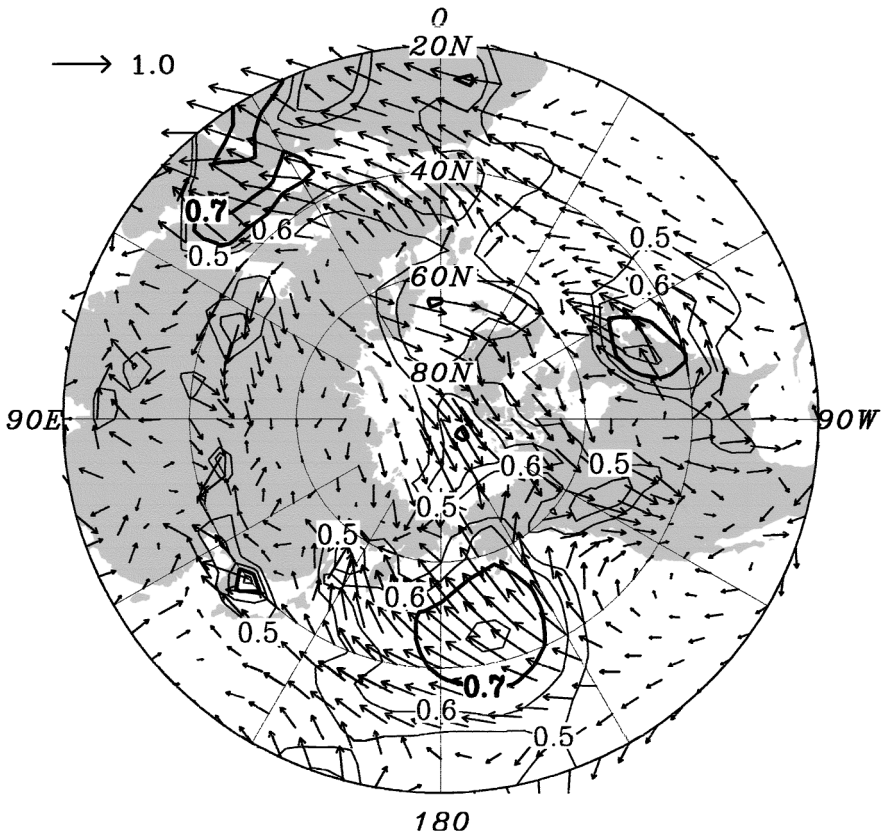

FIG. 16. Same as Fig. 14, but for the decadal second mode.

correlation distribution, combined with the dominant 10–20-yr time scales noted above, indicates that the decadal-to-interdecadal SLP changes of Aleutian low may remotely force the decadal CEOF-2 mode in the Japan Sea. The 10–20-yr variability of the Aleutian low and its relation to the North Pacific were extensively studied in the last decade (e.g., Mann and Park 1996; White et al. 1997; Minobe 1999; Minobe and Nakanowatari 2002; Minobe et al. 2002; Tourre et al. 1999), and is sometimes called the Pacific decadal oscillation (PDO; Mantua et al. 1997), which includes, however, longer-time-scale variability of 50–70- or 20–30-yr-lasting climatic regimes (Minobe 1997, 1999, 2000; Mantua and Hare 2002). The other interesting feature in Fig. 16 is the isolated correlation maximum just over the Japan Sea. This feature cannot be explained by the large-scale atmospheric responses, such as a teleconnection, and hence can be a manifestation of the feedback from the ocean to the atmosphere. However, to confirm the validity of this relatively small-scale correlation pattern and to clarify the meaning of it, it is necessary to examine carefully observational data of SLPs and wind speeds over the Japan Sea in future studies.

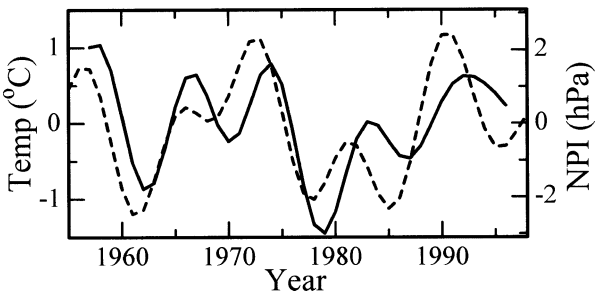

FIG. 17. Same as Fig. 12 but for water temperature reconstructed at 37°N, 135°E and 200-m depth for the decadal CEOF-2 (solid line) and low-pass-filtered wintertime SLPs averaged over the central North Pacific (30°–65°N, 160°E–140°W), which is known as North Pacific index (see text) (dashed line).

A time series comparison reveals covariability between a reconstructed temperature for the action center in the Yamato Basin for the decadal second mode and the wintertime Aleutian low strength, with the reconstructed temperature being delayed to the SLP time series by 1–3 yr (Fig. 17). The SLP time series used here is the North Pacific index (NPI), which is defined as SLP anomalies averaged over 30°–65°N, 160°E–140°W (Trenberth and Hurrell 1994), and is used for a wide range of climate studies over the North Pacific (e.g., Deser et al. 1999; Minobe 2000). One of the major features of the decadal strength changes of Aleutian lows is a climatic regime shift in the 1970s (Nitta and Yamada 1989; Trenberth 1990), which was one of three

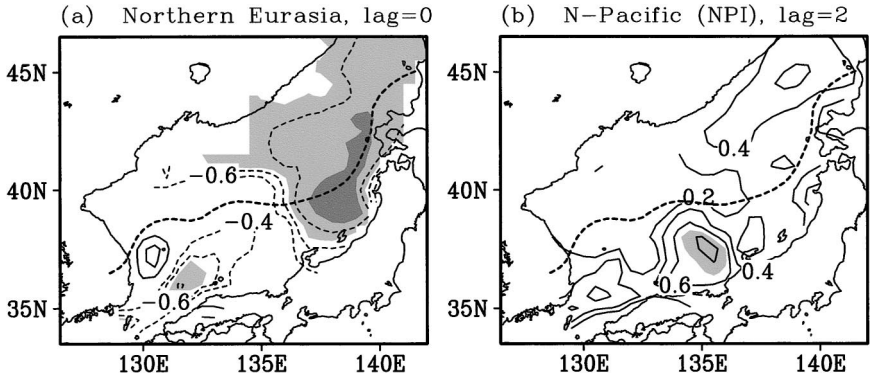

FIG. 18. Lag correlation map of water temperatures at 100-m depth onto the wintertime SLP time series averaged over (a) northern Eurasia and (b) the central North Pacific with the low-pass filtering. The lag in (a) is zero, and the lag for (b) is 2 yr (SLP leading). The SLP time series for (a) and (b) are shown in Figs. 15 and 17, respectively.

major regime shifts in the twentieth century (Minobe 1997, 2000; Mantua et al. 1997). The Japan Sea temperature exhibits a cooling in the 1970s consistent with the regime shift in 1976/77, but the negative temperature anomalies in the 1980s are not as persistent as the negative anomalies of the NPI.

The close relation between the atmosphere and the Japan Sea shown in Figs. 14 and 16 indicates that the first and second modes represent the influence of the decadal variations of Siberian highs and Aleutian lows. This is further confirmed by examining correlation maps of the water temperatures onto the time series of area-averaged SLP over northern Eurasia (Fig. 18a) and the northern North Pacific (Fig. 18b). The SLP time series employed here are those shown by Figs. 15 and 17, respectively. The resultant correlation maps are consistent with the EOF analysis for both the first and second modes, confirming that Siberian highs and Aleutian lows play important roles in the Japan Sea.

7. Discussion and conclusions

In the present paper, we have investigated interannual to interdecadal upper water temperature variations in the Sea of Japan using a new temperature dataset. The temperature dataset was gridded by an optimal interpolation method, from the surface to 400-m depth for a period from 1930 to 1996. The dataset was examined by a CEOF analysis with high-pass (period < 7 yr) or low-pass (period > 7 yr) filters for the latest 40-yr record from 1957 to 1996, and the interannual first mode and the decadal first two modes were closely described.

The interannual first CEOF mode prevails in the upper 200-m depth around and south of the subpolar front in the western Japan Sea, with the dominant periodicity changing from 5–6 yr in the first half of the record to 2–3 yr in the latter half. This periodicity change is consistent with the fact that the earlier papers using the data until the 1970s generally reported about 6-yr oscillations (e.g., Miita and Tawara 1984; Watanabe et al. 1986), but biennial variations were documented by more recent papers (e.g., Isoda 1994; Hirose and Ostrovskii 2000). The correlation analysis between the PC-1 and SLPs suggests that this mode is likely to be forced by the wind anomalies over the Japan Sea in winter, in association with the SLP changes over the western North Pacific.

The change of the dominant time scale from 5–6 to 2–3 yr between the former and latter half of the analysis period may be related with the regime shift in the 1970s. Minobe and Mantua (1999) showed that the interannual variability of the Pacific North American (PNA) pattern [west Pacific (WP) pattern] is strengthened (weakened) after the shift rather than before it. Although they did not examine the dominant time scales of those teleconnection patterns, a visual inspection of their Fig. 8 reveals that the strong WP variability has a relatively longer time scale of around 5–6 yr before the shift, while strong PNA variability has a shorter 2–3-yr time scale after the shift. Therefore, such spatiotemporal structure changes over the western to central North Pacific may affect the interannual variability of the Japan Sea.

The first decadal CEOF mode is characterized by large amplitudes along the subpolar front. Corresponding high correlations of wintertime SLPs are observed over northern Eurasia, suggesting that stronger (weaker) SLP anomalies of northern half of Siberian highs cause an enhanced (weakened) wintertime cooling over the northern Japan Sea, via changing the strength of the east Asian winter monsoon. The decadal fluctuations of the northern Eurasia SLPs are similar to decadal changes of the AO/NAO after 1965. Consequently, the decadal variability of the northeastern Japan Sea is most likely to be dominated by the decadal oscillation of the Siberian high, which is closely related to the decadal variability of the AO/NAO. The phase differences observed between the northeastern and southwestern Japan Sea might be explained by Isoda's (1999) two-box model, but it is necessary to examine his hypothesis with more realistic models in future. Furthermore, it is important

to clarify the mechanism of the possible meridional shift of the subpolar front, which is the most likely to be associated with the temperature anomalies trapped by the front.

The decadal second mode has the localized structure with strong correlations in the Yamato Basin. The corresponding correlation map of wintertime SLPs suggests that this mode is remotely forced by the decadal variability of the Aleutian low over the central North Pacific. The decadal baroclinic Rossby waves propagate from the central North Pacific to the western North Pacific for 4–5 yr (e.g., Deser et al. 1999). The lag of 4–5 yr is slightly longer than the lag of 1–3 yr between the sea level pressures over the central North Pacific and temperatures in the Japan Sea shown in Fig. 17. This suggests that barotropic Rossby waves or local forcings may play a secondary role.

Consequently, the decadal variability of the Japan Sea is primarily influenced by the variability of the Siberian highs, which are related to the AO/NAO, and secondarily by the Aleutian lows, whose decadal variability is closely associated with the PDO. The influence of AO/NAO is also observed in the subsurface water temperature variability in the Okhotsk Sea (Minobe and Nakamura 2004).

The Japan Sea has been recognized as a useful natural experimental sea or a miniature of the World Ocean (Ichiye 1984). The present results show that this is true for studies of interannual to interdecadal variability. Another important topic for the Japan Sea for climate studies may be the substantial reduction of the deep-water formation rate of the JSPW in the middle of the twentieth century (e.g., Nitani 1972; Gamo et al. 2001; Riser et al. 1999), which can be related to the 1940s climatic regime shift over the North Pacific (Minobe 1996), or human influence (Nof 2001), or global warming (Gamo et al. 1986; Kim et al. 2001). The usefulness of the Japan Sea as an experimental ocean for climate studies is not only due to these interesting phenomena, but also due to relatively large numbers of observations even before World War II (Fig. 3).

Acknowledgments. We thank L. D. Talley, S. Martin, and S. Riser for invaluable discussions and anonymous reviewers for their constructive comments. Some figures are produced with the GrADS package developed by B. Doty. This study was supported by grant-in-aid for scientific research, and by a 21st Century Center of Excellence program on ''Neo-Science of Natural History'' lead by H. Okada (to SM) both from the Ministry of Education, Culture, Sports, Science and Technology, Japan.

REFERENCES

Chu, P. C., Y. C. Chen, and S. H. Lu, 1998: Temporal and spatial variabilities of Japan Sea surface temperature and atmospheric forcings. *J. Oceanogr.,* **54,** 273–384.

——, J. Lan, and C. Fan, 2001: Japan Sea thermohaline structure and circulation. Part II: A variational P-vector method. *J. Phys. Oceanogr.,* **31,** 2886–2902.

Deser, C., M. A. Alexander, and M. S. Timlin, 1999: Evidence for a wind-driven intensification of the Kuroshio Current extension from the 1970s to the 1980s. *J. Climate,* **12,** 1697–1706.

Gamo, T., Y. Nozaki, H. Sakai, T. Nakai, and H. Tsubota, 1986: Spatial and temporal variations of water characteristics in the Japan Sea bottom layer. *J. Mar. Res.,* **44,** 781–793.

——, N. Momoshima, and S. Tolmachyov, 2001: Recent upward shift of the deep convection system in the Japan Sea, as inferred from the geochemical tracers tritium, oxygen, and nutrients. *Geophys. Res. Lett.,* **28,** 4143–4146.

Gandin, L. S., 1965: *Objective Analysis of Meteorological Fields.* Israel Program for Scientific Translations, 242 pp.

Gong, D.-Y., S.-W. Wang, and J.-H. Zhu, 2001: East Asian winter monsoon and Arctic Oscillation. *Geophys. Res. Lett.,* **28,** 2073–2076.

Hase, H., J.-H. Yoon, and W. Koterayama, 1999: The current structure of the Tsushima Warm Current along the Japanese coast. *J. Oceanogr.,* **55,** 217–235.

Hirose, N., and A. G. Ostrovskii, 2000: Quasi-biennial variability in the Japan Sea. *J. Geophys. Res.,* **105** (C6), 14 011–14 027.

Hurrell, J. W., 1995: Decadal trends in the North Atlantic Oscillation: Regional temperatures and precipitation. *Science,* **269,** 676–679.

Ichiye, T., 1984: Some problems of circulation and hydrography of the Japan Sea and the Tsushima Current. *Ocean Hydrodynamics of the Japan and East China Seas,* T. Ichiye, Ed., Elsevier, 15–54.

Isobe, A., 1999: On the origin of the Tsushima Warm Current and its seasonality. *Cont. Shelf Res.,* **19,** 117–133.

Isoda, Y., 1994: Interannual SST variations to the north and south of the polar front in the Japan Sea. *La Mer,* **32,** 285–293.

——, 1999: Cooling induced current in the upper ocean of the Japan Sea. *J. Oceanogr.,* **55,** 585–596.

Kalnay, E., and Coauthors, 1996: The NCEP/NCAR 40-Year Reanalysis Project. *Bull. Amer. Meteor. Soc.,* **77,** 437–471.

Kawabe, M., 1982a: Branching of the Tsushima Current in the Japan Sea. Part I: Data analysis. *J. Oceanogr. Soc. Japan,* **38,** 95–107.

——, 1982b: Branching of the Tsushima Current in the Japan Sea. Part II: Numerical experiment. *J. Oceanogr. Soc. Japan,* **38,** 183–192.

Kim, K., and J. Y. Chung, 1984: On the salinity-minimum and dissolved oxygen-maximum layer in the East Sea (Sea of Japan). *Ocean Hydrodynamics of the Japan and East China Seas,* T. Ichiye, Ed., Elsevier, 55–65.

——, K.-R. Kim, D.-H. Min, Y. Volkov, J.-H. Yoon, and M. Takematsu, 2001: Warming and structural changes in the East (Japan) Sea: A clue to future changes in global oceans? *Geophys. Res. Lett.,* **28,** 3293–3296.

Kim, Y.-G., and K. Kim, 1999: Intermediate waters in the East/Japan Sea. *J. Oceanogr.,* **55,** 123–132.

Levitus, S., and Coauthors, 1998: *Introduction.* Vol. 1, *World Ocean Database 1998,* NOAA Atlas NESDIS 18, 346 pp.

Mann, M. E., and J. Park, 1996: Joint spatiotemporal modes of surface temperature and sea level pressure variability in the Northern Hemisphere during the last century. *J. Climate,* **9,** 2137–2162.

Mantua, N. J., and S. R. Hare, 2002: The Pacific decadal oscillation. *J. Oceanogr.,* **58,** 35–44.

——, ——, Y. Zhang, J. M. Wallace, and R. C. Francis, 1997: A Pacific interdecadal climate oscillation with impacts on salmon production. *Bull. Amer. Meteor. Soc.,* **78,** 1069–1079.

Martin, S., and M. Kawase, 1998: The role of the southern flux of sea ice in the Tatarskiy Strait of the Japan Sea in the generation of the Liman Current. *J. Mar. Res.,* **56,** 141–155.

Miita, T., and S. Tawara, 1984: Seasonal and secular variation of water temperature in the East Tsushima Strait. *J. Oceanogr. Soc. Japan,* **40,** 91–97.

Minobe, S., 1996: Interdecadal temperature variation of deep water

in the Japan Sea (East Sea). *Proc. Fourth CREAMS Workshop,* Vladivostok, Russia, CREAMS secretariat, 81–88.
——, 1997: A 50–70 year climatic oscillation over the North Pacific and North America. *Geophys. Res. Lett.,* **24,** 683–686.
——, 1999: Resonance in bidecadal and pentadecadal climate oscillations over the North Pacific: Role in climatic regime shifts. *Geophys. Res. Lett.,* **26,** 855–858.
——, 2000: Spatio-temporal structure of the pentadecadal variability over the North Pacific. *Progress in Oceanography,* Vol. 47, Pergamon, 99–102.
——, and N. Mantua, 1999: Interdecadal modulation of interannual atmospheric and oceanic variability over the North Pacific. *Progress in Oceanography,* Vol. 43, Pergamon, 163–192.
——, and T. Nakanowatari, 2002: Global structure of bidecadal precipitation variability in boreal winter. *Geophys. Res. Lett.,* **29,** 1396, doi:10.1029/2001GL014447.
——, and M. Nakamura, 2004: Interannual to decadal variability in the southern Okhotsk Sea based on a new gridded upper water temperature dataset. *J. Geophys. Res.,* **109,** C09S05, doi: 10.1029/2003JC001916.
——, T. Manabe, and A. Shouji, 2002: Maximal wavelet filter and its application to bidecadal oscillation over the Northern Hemisphere through the twentieth century. *J. Climate,* **15,** 1064–1075.
Naganuma, K., 1985: Fishing and oceanographic conditions in the Japan Sea (in Japanese). *Umi to Sora,* **60,** 89–103.
Nitani, H., 1972: On the deep and bottom waters in the Japan Sea. *Research in Hydrography and Oceanography,* D. Shoji, Ed., Hydrographic Department of Japan Maritime Safety Agency, 151–201.
Nitta, T., and S. Yamada, 1989: Recent warming of tropical sea surface temperature and its relationship to the Northern Hemisphere circulation. *J. Meteor. Soc. Japan,* **67,** 375–383.
Nof, D., 1993: The penetration of Kuroshio water into the Sea of Japan. *J. Phys. Oceanogr.,* **23,** 797–807.
——, 2001: China's development could lead to bottom water formation in the Japan/East Sea. *Bull. Amer. Meteor. Soc.,* **82,** 609–618.
North, G. R., T. L. Bell, R. F. Cahalan, and F. J. Moeing, 1982: Samping errors in the estimation of empirical orthogonal functions. *Mon. Wea. Rev.,* **110,** 699–706.
Ohshima, K. I., 1994: The flow system in the Japan Sea caused by a sea level difference through shallow straits. *J. Geophys. Res.,* **99,** 9925–9940.
Riser, S. C., M. J. Warner, and G. I. Yurasov, 1999: Circulation and mixing of water masses of Tatar Strait and the northwestern boundary region of the Japan Sea. *J. Oceanogr.,* **55,** 133–156.
Senjyu, T., M. Matsuyama, and N. Matsubara, 1999: Interannual and decadal sea-level variations along the Japanese coast. *J. Oceanogr.,* **55,** 619–633.
Sudo, H., 1986: A note on the Japan Sea Proper Water. *Progress in Oceanography,* Vol. 17, Pergamon, 313–336.
Thompson, D. W. J., and J. M. Wallace, 1998: The Arctic Oscillation signature in the wintertime geopotential height and temperature fields. *Geophys. Res. Lett.,* **25,** 1297–1300.
Toba, Y., Y. Tomizawa, Y. Kurasawa, and K. Hanawa, 1982: Seasonal and year-to-year variability of the Tsushima-Tsugaru warm current system with its possible cause. *La Mer,* **20,** 41–51.
Tourre, Y. M., Y. Kushnir, and W. B. White, 1999: Evolution of interdecadal variability in sea level pressure, sea surface temperature, and upper ocean temperature over the Pacific Ocean. *J. Phys. Oceanogr.,* **29,** 1528–1541.
Trenberth, K. E., 1990: Recent observed interdecadal climate changes in the Northern Hemisphere. *Bull. Amer. Meteor. Soc.,* **71,** 988–993.
——, and D. A. Paolino, 1980: The Northern Hemisphere sea-level pressure data set: Trends, errors, and discontinuities. *Mon. Wea. Rev.,* **108,** 855–872.
——, and J. W. Hurrell, 1994: Decadal atmosphere–ocean variations in the Pacific. *Climate Dyn.,* **9,** 303–319.
Uda, M., 1934: The results of simultaneous oceanographic investigations in the Japan Sea and its adjacent waters in May and June (in Japanese). *J. Imp. Fish. Exp. Sta.,* **5,** 57–190.
Watanabe, T., K. Hanawa, and Y. Toba, 1986: Analysis of year-to-year variation of water temperature along the coast of the Japan Sea. *Progress in Oceanography,* Vol. 17, Pergamon, 337–357.
White, W. B., 1995: Design of a global observing system for gyre-scale upper ocean temperature variability. *Progress in Oceanography,* Vol. 36, Pergamon, 169–217.
——, J. Lean, D. R. Cayan, and M. D. Dettinger, 1997: Response of global upper ocean temperature to changing solar irradiance. *J. Geophys. Res.,* **102** (C2), 3255–3266.
Xie, S.-P., H. Noguchi, and S. Matsumura, 1999: A hemispheric-scale quasi-decadal oscillation and its signature in northern Japan. *J. Meteor. Soc. Japan,* **77,** 573–582.
Yoon, J.-H., 1982a: Numerical experiment on the circulation in the Japan Sea. Part I: Formation of the East Korean Warm Current. *J. Oceanogr. Soc. Japan,* **38,** 43–51.
——, 1982b: Numerical experiment on the circulation in the Japan Sea. Part II: Influence of seasonal variations in atmospheric conditions on the Tsushima Current. *J. Oceanogr. Soc. Japan,* **38,** 81–94.
——, 1982c: Numerical experiment on the circulation in the Japan Sea. Part III: Mechanism of the nearshore branch of the Tsushima Current. *J. Oceanogr. Soc. Japan,* **38,** 125–130.